



Article

Influence of Silica Nanoparticles on the Physical Properties of Random Polypropylene

Evangelia Delli ^{1,*}, Dimitrios Gkiliopoulos ², Evangelia Vouvoudi ³, Dimitrios N. Bikiaris ^{3,*}, Thomas Kehagias ⁴ and Konstantinos Chrissafis ¹

¹ Laboratory of Advanced Materials and Devices, Department of Physics, Aristotle University of Thessaloniki, GR-541 24 Thessaloniki, Greece; hrisafis@physics.auth.gr

² Laboratory of Chemical and Environmental Technology, Department of Chemistry, Aristotle University of Thessaloniki, GR-541 24 Thessaloniki, Greece; dgiliopo@chem.auth.gr

³ Laboratory of Polymer Chemistry and Technology, Department of Chemistry, Aristotle University of Thessaloniki, GR-541 24 Thessaloniki, Greece; evouvoud@chem.auth.gr

⁴ Laboratory of Electron Microscopy and Structural Characterization of Materials, Department of Physics, Aristotle University of Thessaloniki, GR-541 24 Thessaloniki, Greece; kehagias@auth.gr

* Correspondence: evdelli@physics.auth.gr (E.D.); dbic@chem.auth.gr (D.N.B.)

Abstract: Random polypropylene is considered an alternative material to regular polypropylene for applications where improved impact and creep resistance, as well as stiffness, are required. Random polypropylene nanocomposites reinforced with dimethyldichlorosilane-treated silica particles were prepared using meltmixing. The effect of varying the nanoparticles' content on the structural, mechanical, damping and thermal behavior of the nanocomposites was investigated. The results indicated the improved deformation potential, fracture toughness, and energy storage capacity of the matrix with increasing the filler content. It was observed that the use of high filler fractions limited the reinforcing efficiency of the SiO₂ nanoparticles due to the formation of large agglomerates. The nanoparticles' segregation was initially advised by modeling Young's modulus but was also confirmed by electron imaging. Examination of the thermal properties of the nanocomposites indicated the limited effect of the nanoparticles on the melting behavior along with the thermal stability of the matrix. These results confirmed the usage of silica nanoparticles as a way of further improving the mechanical and thermomechanical properties of random polypropylene.

Keywords: nanocomposites; silica nanoparticles; thermal properties; mechanical properties; DMA



Citation: Delli, E.; Gkiliopoulos, D.; Vouvoudi, E.; Bikiaris, D.N.; Kehagias, T.; Chrissafis, K. Influence of Silica Nanoparticles on the Physical Properties of Random Polypropylene. *J. Compos. Sci.* **2024**, *8*, 186. <https://doi.org/10.3390/jcs8050186>

Academic Editor: Francesco Tornabene

Received: 10 April 2024

Revised: 8 May 2024

Accepted: 14 May 2024

Published: 16 May 2024



Copyright: © 2024 by the authors. Licensee MDPI, Basel, Switzerland. This article is an open access article distributed under the terms and conditions of the Creative Commons Attribution (CC BY) license (<https://creativecommons.org/licenses/by/4.0/>).

1. Introduction

Polymeric composite materials, consisting of a polymeric matrix and a disperse phase, have reached a high variation level and demonstrated a continuously grown commercial interest for applications in industrial fields, such as automotive, renewable energies, aircraft and construction [1]. A large variety of reinforcing agents can be used as dispersed material, scaling from the nano- to macro-dimensions, enabling the tailoring of the properties of the polymer and resulting in superior physical and chemical characteristics. Glass-reinforced polyesters stand as the most typical example of industrially used polymeric composites for which the filler component allows the enhancement of the hardness, strength and stiffness of the polymeric matrix [2,3]. However, such composites often face limitations related to the processability and the effectiveness of the final product, which strongly depends on the interfacial adhesion between the polymer and the filler. Low-strength bonding between the organic polymer and the inorganic reinforcing agent leads to the formation of easy fracture points that can greatly deteriorate the performance of the composite, as the mechanical load cannot be transferred to the strong filler component [4]. Alternatively, more technologically advanced nano-fillers with a size of the order of a few nanometers and high surface-to-volume ratio values (200–1000) can be used, something that greatly

affects the interfacial adhesion and the mechanical properties [5,6]. Presently, metal oxides (ZnO, TiO₂, Al₂O₃), SiO₂ and carbon nanoparticles (NPs) have been widely used as fillers, demonstrating profound effects on the mechanical, thermal and chemical properties of the polymeric matrix [7,8].

The prospect of reinforcing polymers, such as polyethylene (PE) and polypropylene (PP), using metalloid oxides, such as silica (SiO₂), has resulted in nanoparticles being broadly studied mainly due to their easy preparation process, which maintains the relatively low fabrication cost of the composites [5]. Furthermore, varying the ratio of the components used in the synthesis of SiO₂ NPs allows customizing the nanoparticles' morphology, leading to shapes such as porous spheres, ribbons, tubes, cubes, etc. [9]. This greatly affects the final properties of the particles, which, in turn, allows for broadening the range of applications. Simulations have also shown that SiO₂ NPs can greatly affect the mechanical and tribological properties of the composites due to the strong interaction of the nanoparticles with the polymer chains [10]. Silica-reinforced polypropylene has indeed demonstrated enhanced yield stress and impact strength compared to the pure polypropylene matrix, mainly due to the improved crack propagation resistance of the nanoparticle/matrix interface [11]. Additionally, the incorporation of up to 5 wt.% SiO₂ nano-fillers can improve the thermal stability of the PP matrix [12].

Compounding polypropylene with different monomers, such as ethylene and octane, has also been seen to improve the mechanical properties of PP [13]. Copolymerization drastically affects the microstructure of the matrix, as the monomer units are randomly dispersed in the PP chains [14]. The copolymerization of polypropylene with small quantities of ethylene leads to a copolymer widely known as polypropylene random (PP_R). Compared to simple polypropylene homopolymers, PP_R is characterized by improved impact resistance, aging and heat tolerance, making it suitable for harsh environment applications, such as hazardous chemical solutions and water pipeline systems [15]. Recently, it was reported that the addition of 5 wt.% fumed silica nanoparticles in a PP_R matrix using the melting extrusion process greatly enhances the crystallization temperature, the thermal stability and Young's modulus of the matrix [16]. However, not much work has been focused on the effect of SiO₂ NP content on the physical properties of PP_R, and this is a visible novelty in relation to the literature.

In this work, SiO₂ nanoparticles were used to reinforce the mechanical and thermal characteristics of the PP_R matrix. The nanoparticle-reinforced PP_R composites were prepared using meltmixing. Previous reports suggest that high-volume fractions of silica nanoparticles lead to NP agglomerations, which greatly deteriorated the mechanical performance of the composites. Thus, the filler content varied from 1% to a maximum value of 10 wt.%. Differences in the thermal, mechanical and thermomechanical properties of the nanocomposites with the varying silica nanoparticle weight fractions are discussed. The incorporation of organically treated nanoparticles in the random polypropylene matrix allows for the formation of some interfacial bonds, which greatly improve the elasticity, toughness and stiffness of the matrix. The thermal degradation only demonstrated a significant improvement with the addition of 10 wt.% NPs, while the melting and cooling behavior of all nanocomposites was similar to that of pure PP_R.

2. Materials and Methods

2.1. Materials Applied

The random polypropylene material used had a density of approximately 0.7 g/cm³ and was provided by Interplast S.A (Komotini, Thrace, Greece) in the form of granules and consisted of 7 wt.% ethylene and 93 wt.% propylene. The silica nanoparticles (AEROSIL® R 972) are fumed silica after treated with dimethyldichlorosilane in the form of a fine powder with a nominal surface area of 110 m²/g and were purchased by Evonik (Essen, Germany). Four SiO₂-reinforced PP_R composites were created with 1, 2.5, 5, and 10 wt.% of silica nanoparticles using a co-rotating, twin screw roller blade Haake-Buchler mixer (Maake Buchler Instruments Inc., Saddle Brook, NJ, USA). The nanoparticles and the PP_R granules

were meltmixed together at 190 °C using a rotation speed of 30 rpm and a total time of 15 min. No drying process was performed on the silica NPs prior to their melt mixing with the PP_R matrix, and they were stored in a dry and dark place. Following mixing, the melts were left to reach room temperature (RT) and chopped manually into granules.

2.2. Characterization Methods

The structure of the composites was tested using a Perkin-Elmer Spectrum 100 infrared (IR) spectroscope and a two-circle Rigaku Ultima⁺ diffractometer, which was equipped with a Cu-K α X-ray radiation source. The IR spectra were obtained using 32 scans and a resolution of 4 cm⁻¹. For both characterization techniques, suitable thin polymer films were prepared using a Paul-Otto Weber type PW 30 hydraulic press operating at 190 °C, which was controlled by an Omron E5AX Temperature Controller. The thin films were prepared by hot pressing some polymer granules for 2 min using a pressure of 80 kN. The thickness of the films used for the X-ray diffraction (XRD) characterization was approximately 20 nm, while the films tested using infrared transmittance had a thickness of approximately 10 nm. The IR spectra of the SiO₂ NPs were obtained using a KBr pellet with a composition in SiO₂ of 1 to 2 wt.% for better beam penetration.

A Netzsch Differential Scanning Calorimetry (DSC) 214 Polyma instrument was used to test the melting and cooling behavior of neat PP_R and the composites. The thermograms were obtained by heating and cooling the sample using a rate of 20 °C/min under a nitrogen flow of 60 mL/min (>99.9%). All specimens underwent the same thermal history erase procedure prior to the heating and cooling test.

Thermogravimetric measurements were performed using a TG/TDA Setaram Setsys 16/18 instrument. The samples were heated from room temperature up to 700 °C using a rate of 20 °C/min under a nitrogen flow of 20 mL/min (>99.9%).

Tensile testing of dumbbell-shaped specimens (length: 38 mm and width: 1.6 mm) prepared for each sample was performed following the ASTM D638 standard using an Instron Model 3344 2kN capacity Dynamometer. The dynamometer was controlled by Instron Bluehill software for Windows 2000 while applying a crosshead speed of 50 mm/min. The hot press was employed to melt the polymeric granules and form films of approximately 1 mm thickness. The dumbbell-shaped specimens were created using a Wallace S1 cutting press operated by hand. Five specimens were prepared for each sample and stressed, which allowed us to obtain the average values for Young's modulus, yield strength and stress at the breakpoint. The elongation at the break was calculated using the maximum stress.

Dynamic mechanical analysis (DMA) was performed using a PerkinElmer Diamond DMA. DMA-suitable rectangular specimens (span length, 40 mm, width, 12 mm and height, 4 mm) for each composite were formed using the hot press apparatus and suitable metallic molds. All specimens were tested over the temperature range of 25 to 110 °C using a 3 °C/min heating rate, a bending force of 4000 mN and an oscillation frequency of 1 Hz. During DMA testing, N₂ (>99.9%) was purging the oven constantly using a flow rate of 20 mL/min.

The fracture toughness of the nanocomposite was tested using the single-edge notched method. Suitable specimens with a length of 55 mm, a width of 2.5 mm and a height of 10 mm were formed again using the hot press and suitable metallic molds. The notch had a depth of 2.5 mm.

Scanning electron microscopy (SEM) imaging of the fracture surfaces of the specimens' tensile stresses was collected using a JEOL JSM 840A-Oxford ISIS 300 SEM operated using 20 kV. The morphological features of selected nanocomposites were investigated by Transmission Electron Microscopy (TEM) using a Jeol JEM 1010 electron microscope operated at 100 kV. TEM specimens were prepared by sectioning the samples in a Leica UCT Ultracut ultramicrotome and collecting thin sections on 400-mesh Au grids.

3. Results and Discussion

Transmittance spectra of the polymers, as well as SiO₂ NPs, are shown in Figure 1a. The spectra of the NPs demonstrated broad range wavenumber peaks due to the amorphous phase of the nanoparticles. The peaks are related to the asymmetric stretching vibration of the Si-O-Si bonds (~1100 cm⁻¹), the bending vibration (~812 cm⁻¹) and the rocking vibration of Si-O (~472 cm⁻¹) [17]. Well-defined IR peaks were observed in the spectra of the neat PPR sample. These peaks are attributed to the vibrations of the PPR matrix polymer chain and side groups. Specifically, the peaks are assigned to the symmetric (~1377 cm⁻¹) and non-symmetric (~1460 cm⁻¹) bending of -CH₃, stretching of C-C, bending of -CH (~1167 cm⁻¹), wagging of -CH₂ (~997 cm⁻¹), and the rotation of -CH₂ (~841 cm⁻¹) and -CH₃ (~973 cm⁻¹) [18]. Similar peaks were also observed for the spectra of all the PPR/SiO₂ nanocomposites alongside the wide peak attributed to the stretching vibration of the Si-O-Si bonds in the NPs. Furthermore, increasing the SiO₂ NP content in the PPR matrix led to a substantial increase in the Si-O-Si stretching vibration peak.

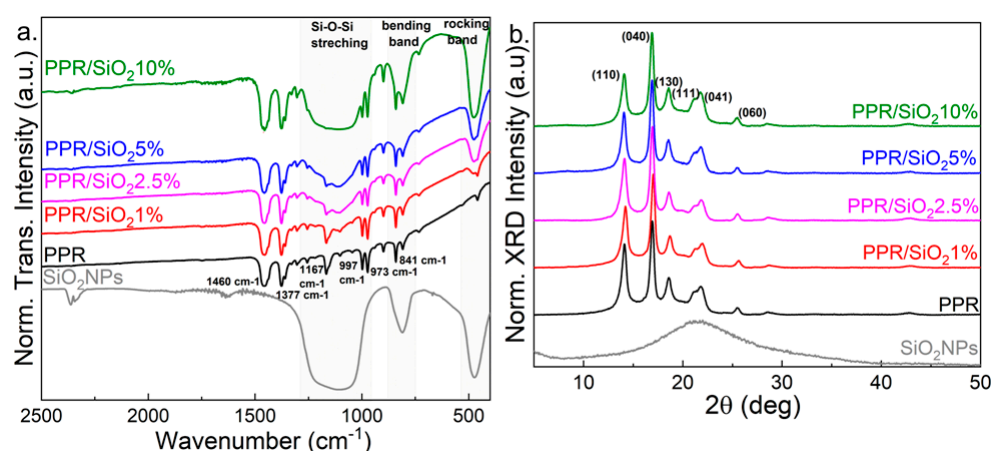


Figure 1. Structural characterization: (a) FT-IR transmittance spectrum and (b) X-ray diffraction pattern of the SiO₂ NP composites, neat PPR, and SiO₂ nanoparticles.

The amorphous state of the SiO₂ nanoparticles, as well as the semicrystalline state of the neat PPR and the PPR/SiO₂ nanocomposites, was also confirmed using X-ray diffraction (XRD). The corresponding XRD patterns are shown in Figure 1b. Characterization of the NPs indicated a wide peak centered at a 2θ angle of 21 degrees associated with the diffraction from the amorphous SiO₂. All nanocomposites, as well as neat PPR, demonstrated the same strong diffraction peaks at around 14.1, 16.8, 18.4, 21.2, and 25.5 degrees attributed to diffraction from the (110), (040), (130), (111), (041) and (060) crystallographic planes. These diffraction planes are characteristic of an α-crystal phase of PP. There was not a significant effect on the shape of the diffractograms with increasing the NP filler content in the PPR matrix. Furthermore, as shown in Table 1, the additions of SiO₂ did not interrupt the formation of polymer lamella crystallites. The thickness of the polymer crystallites perpendicular to the diffraction crystal planes of interest was obtained using the XRD patterns and the Debye–Scherrer equation [19] as follows:

$$L_{xkl} = \frac{\kappa \cdot \lambda}{b \cdot \cos \theta} \quad (1)$$

where $\lambda = 0.15418$ nm is the wavelength of the X-rays used to obtain the diffraction patterns, $\kappa = 0.9$ is the shape factor, b is the full width at half maximum, and θ is the angle of the diffraction peaks. The diffraction angle and b were in radians. Overall, all samples demonstrated similar crystallite sizes perpendicular to the diffraction planes. However, the lateral size L_{110} is slightly reduced with the addition of NPs compared to plain PPR, indicating that the silica particles disturb the formation of the crystals [11].

Table 1. XRD crystalline structure characteristics of PP_R and PP_R/SiO₂ nanocomposites. L_{xkl} is the thickness of polymeric crystallites perpendicular to the (xkl) crystal planes, where x, k, l = 0, and 1 are the Miller indices of the planes.

Sample	L ₍₁₁₀₎ (nm)	L ₍₀₄₀₎ (nm)
PP _R	14.6	18.7
PP _R /SiO ₂ 1%wt	14.5	18.9
PP _R /SiO ₂ 2.5%wt	13.0	18.9
PP _R /SiO ₂ 5%wt	14.0	19.7
PP _R /SiO ₂ 10%wt	14.0	18.4

The thermal properties of the samples were investigated using differential scanning calorimetry and thermogravimetry, and the results are shown in Figure 2. Pure PP_R demonstrated a single peak in the heating and cooling thermogram, peaking at around 147 °C and 93 °C, respectively, which is due to the melting and crystallization of PP_R *a*-phase crystallites. These temperatures are considerably lower compared to those reported in the literature for pure PP [12,20], as a result of propylene and ethylene copolymerization. The polymer nanocomposites also show the same melting and cooling behavior. The melting peak, T_m, demonstrated a small shift towards lower temperatures upon increasing the silica NP content (Table 2) which can be attributed to a limited decrease in the thickness of the polymeric lamella [12]. It should be noted that polymer crystallinity was calculated using the actual weight fraction of the SiO₂ based on the TGA residual mass results found. Crystallinity is in good agreement with the results obtained by the analysis of XRD peaks. Comparing the nanocomposites' behavior to that of PP_R, the crystallization temperature, T_c, also increased slightly, suggesting that the NPs may act as nucleation sites. However, the influence of the silica nanoparticles is very low and does not manifest a distinct dependence on the filler content. Furthermore, analysis of the melting enthalpy of the polymers suggested that, in fact, NP interfere with the lamella crystallization as the degree of crystallinity reduced with increasing the SiO₂ content. The degree of crystallinity, X_c, of all polymers was calculated using the melting enthalpy and the following equation [21]:

$$X_c = \frac{\Delta H_m}{(1 - w) \cdot \Delta H_m^0} \cdot 100\% \quad (2)$$

where ΔH_m and ΔH_m⁰ = 207 J/g [22] are the melting enthalpy of the samples and 100% crystalline PP_R, correspondingly. The weight fraction, *w*, of the NPs in the composites was also considered.

Table 2. DSC and TGA characterization results obtained for neat PP_R and the various PP_R/SiO₂ nanocomposites using a temperature change rate of 20 °C/min. It should be noted that polymer crystallinity was calculated using the actual weight fraction of the SiO₂ based on the TGA residual mass results found.

Sample	T _m (°C)	T _c (°C)	ΔH _m (J/g)	X _c (%)	T _{5%} (°C)	T _{10%} (°C)	m _{res} (%)
PP _R	147.1	93.2	62.4	30.2	421.3	436.7	0
PP _R /SiO ₂ 1%wt	147.6	92.8	60.5	29.5	421.1	438.6	1.6
PP _R /SiO ₂ 2.5%wt	147.1	94.1	58.2	28.8	415.0	432.5	2.8
PP _R /SiO ₂ 5%wt	146.7	93.5	55.7	28.3	419.4	436.2	5.0
PP _R /SiO ₂ 10%wt	146.1	93.9	55.7	29.3	423.2	441.7	8.0

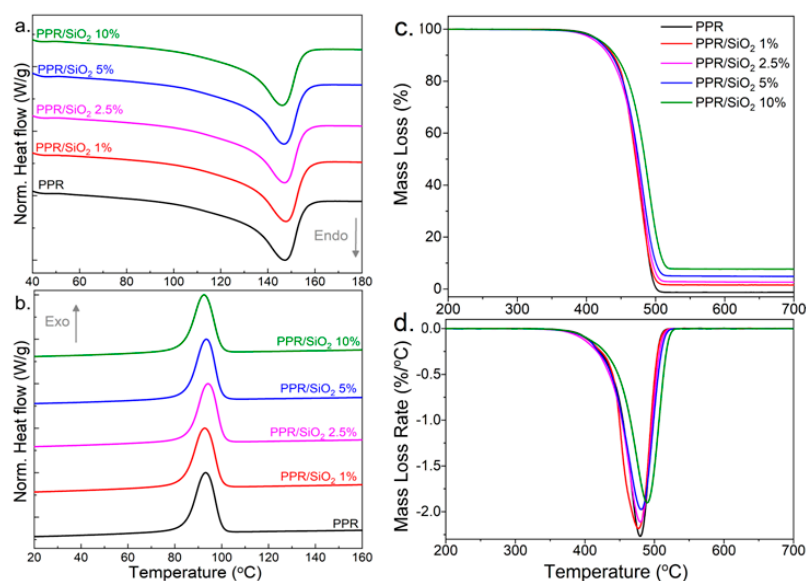


Figure 2. Thermal characterization: thermograms recorded during (a) DSC heating and (b) DSC cooling of PPR and its nanocomposites, while (c) TGA weight loss curves of all samples pyrolyzed and (d) the derived curves of the mass loss rate are also illustrated.

Figure 2c also shows the thermal stability results obtained for all samples under N₂ flow. The temperature of 5% and 10% mass loss, as well as the residue SiO₂ NP weight, are reported in Table 2. The weight loss curves of neat PPR and the nanocomposites demonstrated a similar shape, which are typical of the degradation curve of PP. As the SiO₂ NPs have excellent thermal stability over the degradation temperature range used, it is believed that the residual mass is attributed to the presence of the SiO₂ NPs. Analysis of the residual mass obtained for all degradation curves suggests a good control over the composition of the nanocomposites and dispersion of the NPs for a filler content of up to 5 wt.%. The nanocomposites with the higher filler content had a significantly lower residual mass (8%) compared to the theoretical values (10%). This is due to the inability of the PPR matrix to fully accumulate the NPs added during the melting mixing procedure. While removing the mold from the extruder, it was observed that for the same melting time as the rest of the nanocomposites, an accountable amount of powder was not successfully incorporated into the matrix. Furthermore, analysis of the TGA curves indicated that the nanoparticles had a moderate effect on the thermal stability of the polymer matrix. The highest thermal stability was observed for the composite with the maximum filler content. For the nanocomposite PPR/SiO₂ 10 wt.% (8 wt.% real value), the T_{5%} and T_{10%} temperature were approximately 2 and 5 °C higher compared to that of PPR. On the contrary, adding only 1 wt.% SiO₂ NPs did not affect the T_{5%} temperature. Furthermore, as shown in the inset figure in Figure 2, the samples had a similar maximum rate degradation temperature, excluding PPR/SiO₂ 10 wt.%, which had a degradation temperature 10 °C higher (489.5 °C) than pure PPR (479.5 °C).

Next, the mechanical strength of the polymers was tested using strain–stress and impact strength characterization techniques, and the results are shown in Figure 3. The elastic modulus, *E*, of the nanocomposites significantly increased with increasing the filler content, reaching a maximum value of 459 ± 16 MPa, which is approximately 2.4 times higher compared to that of PPR. According to the literature, the rise of the modulus is related to the strong interaction between the NPs and the polymeric matrix and the presence of an interphase formed in between. The interphase improves the stress transfer from the PPR matrix to the highly stiff silica nanoparticles, allowing the accommodation of

higher stress loads [23]. The elastic modulus of the nanocomposites was modeled using the Einstein model [24] (Figure 3a) and the following equation:

$$E_{NC} = E_m (1 + 2.5 \cdot V_f) \tag{3}$$

where V_f is the filler volume fraction given by

$$V_f = \left(1 + \frac{\rho_f}{\rho_m} \frac{1 - w}{w} \right)^{-1} \tag{4}$$

ρ_m and $\rho_f = 0.05 \text{ g/cm}^3$ are the density of the matrix and SiO_2 NP nanoparticles, respectively. The volume fraction values used in the model were obtained using the actual filler content obtained by the TGA results analysis. For nanoparticles with real content up to 2.8 wt.%, the elastic modulus dependence on the filler is perfectly described by the Einstein model. The addition of 1 wt.% and 2.5 wt.% (1.6 wt.% and 2.8 wt.% real value) silica NPs increased the modulus to $295 \pm 33 \text{ MPa}$ and $3234 \pm 20 \text{ MPa}$, respectively. However, a further increase in the NP weight fraction resulted in modulus values being significantly lower compared to those expected by the Einstein model. This could be due to the reduction in the silica dispersion/homogenation in the PP_R matrix and the formation of big agglomerates as the NP content increases. The yield stress of the nanocomposites was also significantly higher than that of PP_R . Interestingly, even the nanocomposites with the higher filler fraction demonstrated an improved yield stress despite the agglomeration formation. This suggests that yielding mostly depends on an increase in the stiffness and the restricted motion of the polymer chain segment rather than the filler dispersion [25]. Furthermore, the improved yield strength is accompanied by a reduction in the maximum elongation of the specimens before breakage, probably due to the agglomerated formation and the limited chain motion.

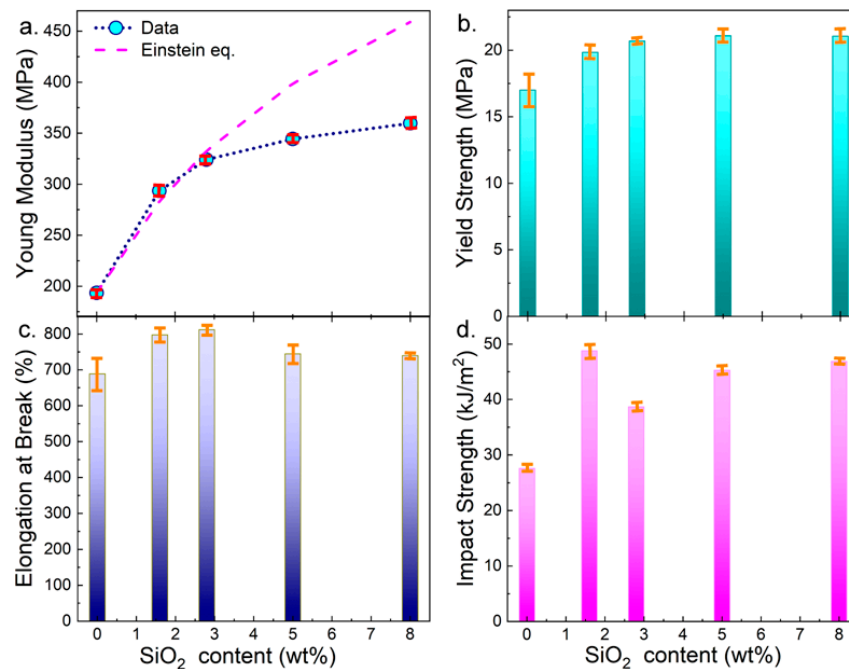


Figure 3. Mechanical characterization: effect of SiO_2 NP content on (a) Young’s modulus of the nanocomposites. The data were fit using the Einstein model. (b) Tensile strength, (c) elongation at break results, and (d) impact toughness as a function of the nanoparticles content. The SiO_2 NP content values used are based on those obtained from the actual TGA analysis of each sample. The presented data correspond to the average values obtained out of five specimens tested for each composition, while error bars indicate the standard deviation.

The addition of SiO₂ NPs led to significantly higher impact strength compared to the pure PP_R matrix, as shown in Figure 3c. This confirms the formation of an intermedium phase between the polymeric matrix and the NPs, which increases the debonding resistance and lowers the probability of the polymer being separated from the filler. In this way, the nanocomposites were able to withstand a higher impact load before breaking while resisting the propagation and formation of cracks [12]. However, for SiO₂ content higher than 1 wt.% (1.6 wt.% real value), the impact strength demonstrates lower values. This indicates the formation of agglomerates, which leads to matrix “de-wetting” and reduces the strength of the nanocomposites.

Micrographs of the fracture area of the specimens used during the strain–stress characterization were obtained by SEM, and they are shown in Figure 4. Pure PP_R had a smooth and brittle fractured surface. The addition of silica NPs in the PP_R matrix led to a more fibrillar surface attributed to the enhancement of plastic deformation of the matrix. The inset figures are images obtained with higher magnification, allowing better observation of the fracture surface. Small SiO₂ NP aggregates were observed for filler content of 5 wt.% and 10 wt.% (8 wt.% real value), confirming the previous mechanical analysis results.

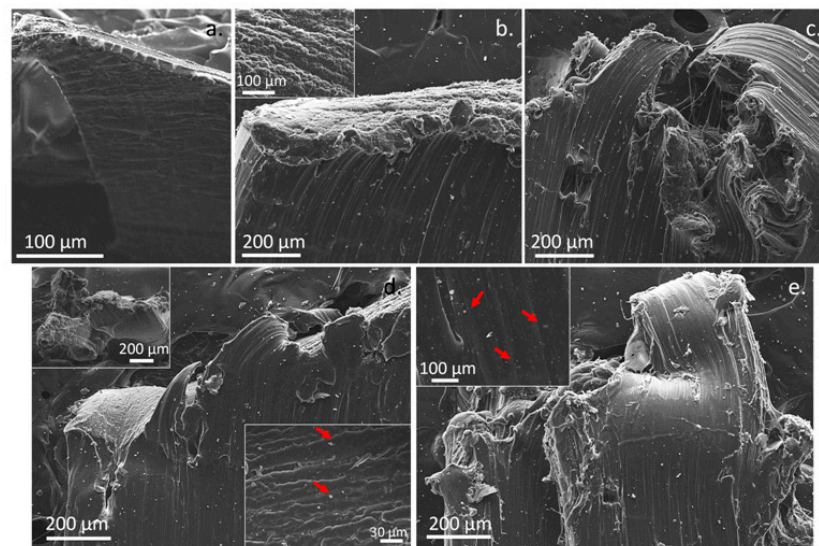


Figure 4. SEM imaging of the PP_R/SiO₂ nanocomposites. Images of the fracture area of dumbbell-shaped specimens obtained for (a) neat PP_R and its nanocomposites with (b) 1 wt.%, (c) 2.5 wt.%, (d) 5 wt.%, and (e) 10 wt.% SiO₂ NPs. The red arrows indicate the position of SiO₂ nanoparticle agglomerations.

The formation of agglomerates was further investigated for the two outermost values of the filler content, namely, the 1% and the 10 wt.%, using TEM (Figure 5). The nanocomposite with the lowest NP weight fraction demonstrated a rather uniform dispersion of small NP aggregates, with sizes varying from 75 to 130 nm (Figure 5a). Increasing the filler content to 10 wt.% led to the formation of significantly larger agglomerates of more than 500 nm in length, exhibiting an irregular distribution (Figure 5b).

Finally, the thermomechanical properties of the nanocomposites were investigated using DMA. Figure 6 shows the dependence of the storage modulus, E' , and $\tan\delta$ as a function of temperature obtained using a frequency of 1 Hz. All samples demonstrated an analogous E' dependence on temperature, which is characteristic of the PP polymer and its composites [26]. The nanocomposites showed significant improvement in the storage modulus with an increase in the SiO₂ NP weight fraction throughout the studied temperature range. Despite the agglomeration's formation, maximum modulus values were obtained for the nanocomposites with the higher SiO₂ composition. Overall, the addition of NPs led to higher $\tan\delta$ values for temperatures higher than 80 °C, owing to the nanoparticles' dispersion on the matrix, which limits the crystallinity compared to

neat PPR [26]. The nanocomposites with only 1 wt.% silica NPs demonstrated an elastic character in the low-temperature range and a “vibration” damping efficiency, like that of pure PPR for temperatures above 80 °C. Similarly, improved elastic behavior was also observed for the nanocomposite PPR/SiO₂ 10 wt.% in the temperature range of 40 to 80 °C.

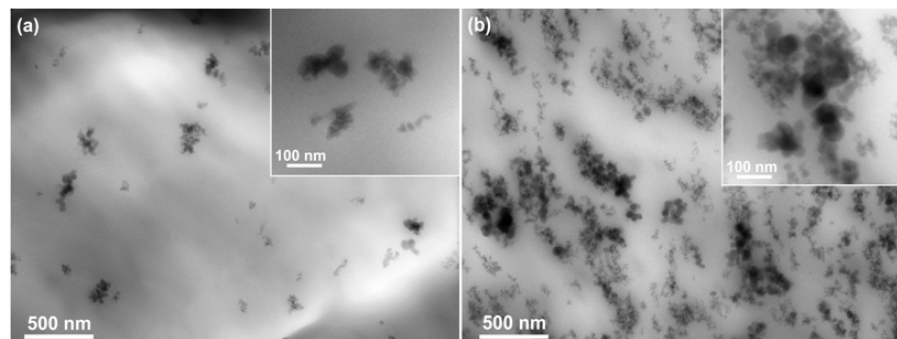


Figure 5. TEM imaging of the PPR/SiO₂ nanocomposites: bright field micrographs of (a) PPR/SiO₂ 1 wt.% and (b) PPR/SiO₂ 10 wt.% nanocomposites. The insets show magnified images of the nanoparticles' aggregates in the polymeric matrix for the two cases, respectively.

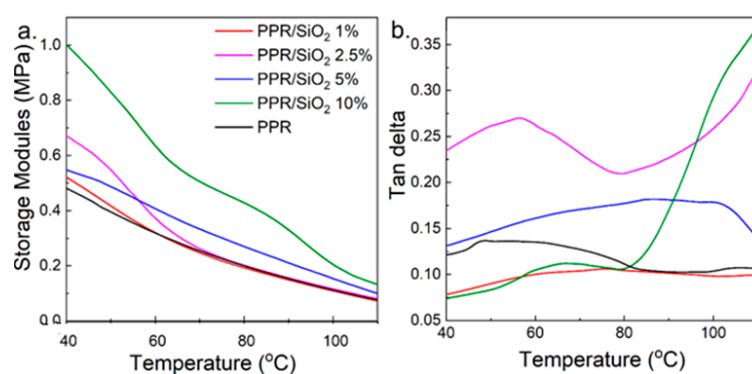


Figure 6. DMA characterization: (a) storage modulus E' and (b) $\tan\delta$ curves of neat PPR and the PPR/SiO₂ composites as a function of temperature.

Last, it could be stated that the potential limitation of this work lies in the low chemical affinity that the silica shows with the polyolefins. The SiO₂ is hydrophilic, while the PP is highly hydrophobic; yet, the best that could be arranged in this study was applied, i.e., the silica particles were organically treated before incorporation, the particles were ranged in nanoscale, and low concentrations were elaborated for homogenous applications. Plus, a careful meltmixing process was elaborated for satisfactory incorporation (in time/temperature conditions).

4. Conclusions

All in all, SiO₂ silane-treated nanoparticles actually reinforced PPR composites with up to 10 wt.% filler content, which was prepared by meltmixing. It was found that concentrations of 2.5 or 5 wt.% were generally satisfactory in most tests/analyses applied; thus, they are proposed for “real-life” applications. Thermogravimetry indicated the inability of PPR to fully absorb 10 wt.% SiO₂, while for lower filler fraction, a good agreement between the theoretical weight fraction and the residual SiO₂ mass was obtained. Improved thermal degradation was only observed for the nanocomposite with the highest content of nanoparticles. Low silica concentration (<5 wt.%) led to an increase in the mechanical properties of the composite. However, a further increase in the filler concentration resulted in the formation of large agglomerates, which hinder the NPs' reinforcing efficiency and lower the breakage and impact resistance of the matrix. A maximum impact strength

of 49 kJ/m² was obtained for PP_R/SiO₂ 1 wt.% nanocomposites, a value approximately 1.8 times higher compared to that of pure PP_R. Analysis of the strain–stress elongation results indicated a steady increase in the yield strength and Young’s modulus. However, by increasing the filler content above 2.5 wt.%, the prediction suggested a much higher Young’s modulus compared to the experimental data. This deviation was explained by the formation of NP agglomerates, which hinders the improvement of the mechanical properties. SEM and TEM imaging of the samples also confirmed the presence of large aggregations for high NP weight fractions. Finally, the addition of silica nanoparticles greatly affected the storage modulus due to the satisfactory adhesion between the PP_R matrix and the nanoparticles. Particularly, all nanocomposites demonstrated an improved energy storage capacity compared to pure PP_R in the temperature range from 40 to 80 °C. The NPs’ successful incorporation and crystal state of the nanocomposites were confirmed by FT-IR and XRD. The formation of a stronger, wider peak in the IR spectra attributed to the Si-O-Si bond stretching vibrations with increasing the filler content clearly confirmed the incorporation of the nanoparticles. Analysis of the XRD patterns did not indicate any clear effect on the lamella crystallization, which was also confirmed by the DSC results. Particularly, the melting and cooling temperatures did not show any great dependence on the nanoparticle content. This sum of results confirmed the reinforcing effect of silica NPs on the mechanical and damping properties of the PP_R while preserving the thermal characteristic of the matrix. This indicates the potential use of PP_R/SiO₂ nanocomposites for a broad range of applications for which improved mechanical performance is required without significantly affecting thermal stability, such as water supply pipelines and heating pipe systems.

Author Contributions: Conceptualization, K.C., D.N.B. and E.D.; methodology, E.D. and D.G.; software, E.D.; investigation, E.D., E.V., T.K. and D.G.; data curation, E.D. and T.K.; writing—original draft preparation, E.D. and E.V.; writing—review and editing, D.N.B.; visualization, E.D.; supervision, K.C. and D.N.B.; funding acquisition, K.C. and D.N.B. also served as scientific advisors. All authors have read and agreed to the published version of the manuscript.

Funding: This work was financially supported by Greek national funds and the Regional Development Fund of the European Union through the operational program Competitiveness, Entrepreneurship, and Innovation (research call RESEARCH—CREATE—INNOVATE, project code T1EDK-02575).

Data Availability Statement: The original contributions presented in the study are included in the article material, further inquiries can be directed to the corresponding authors.

Acknowledgments: The authors would like to thank C. Papoulia, E. Pavlidou, and T. Zorba for their support.

Conflicts of Interest: The authors declare no conflicts of interest.

References

1. Zindani, D.; Kumar, K. Chapter 1: Industrial applications of polymer composite materials. In *Composites and Advanced Materials in Industrial Applications*; IGI Global: Hershey, PA, USA, 2018.
2. Harmia, T.; Hartikainen, J.; Lindner, M. Long fiber-reinforced thermoplastic composites in automotive applications. In *Polymer Composites: From Nano- to Macro- Scale*; Harmia, T., Ed.; Springer: Boston, MA, USA, 2005; pp. 256–262.
3. Mohan Kumar, S.; Raghavendra Ravikiran, K.; Govindaraju, H.K. Development of E-Glass woven fabric/polyester resin polymer matrix composite and study of mechanical properties. *Mater. Today Proc.* **2018**, *5*, 13367–13374. [[CrossRef](#)]
4. Huang, S.; Fu, Q.; Yan, L.; Kasal, B. Characterization of interfacial properties between fibre and polymer matrix in composite materials—A critical review. *J. Mater. Res. Technol.* **2021**, *13*, 1441–1484. [[CrossRef](#)]
5. Mallakpour, S.; Naghdi, M. Polymer/SiO₂ nanocomposites: Production and applications. *Prog. Mater. Sci.* **2018**, *97*, 409–447. [[CrossRef](#)]
6. Morimune-Moriya, S.; Goto, T.; Nishino, T. Effect of aspect ratio of graphene oxide on properties of poly(vinylalcohol) nanocomposites. *Nanocomposites* **2019**, *5*, 84–93. [[CrossRef](#)]
7. Ponnamm, D.; Cabibihan, J.-J.; Rajan, M.; Pethaiah, S.S.; Deshmukh, K.; Gogoi, J.P.; Pasha, S.K.K.; Ahamed, M.B.; Krishnegowda, J.; Chandrashekar, B.N.; et al. Synthesis, optimization and applications of ZnO/polymer nanocomposites. *Mater. Sc. Eng. C* **2019**, *98*, 210–240. [[CrossRef](#)] [[PubMed](#)]

8. Moniruzzaman, M.; Winey, K.I. Review- Polymer Nanocomposites Containing Carbon Nanotubes. *Macromolecules* **2006**, *39*, 5194–5205. [[CrossRef](#)]
9. Li, D.M.; Chen, Y.C.; Zhang, C.; Song, S.; Zheng, Y.S. Different morphologies of silica synthesized using organic templates from the same class of chiral compounds. *J. Mater. Chem. B* **2013**, *1*, 1622. [[CrossRef](#)] [[PubMed](#)]
10. He, E.; Wang, S.; Li, Y.; Wang, Q. Enhanced tribological properties of polymer composites by incorporation of nano-SiO₂ particles: A molecular dynamics simulation study. *Comput. Mater. Sci.* **2017**, *134*, 93–99. [[CrossRef](#)]
11. Garcia, M.; Van Vliet, G.; Jain, S.; Schrauwen, B.A.G.; Sarkissov, A.; Van Zyl, W.E.; Boukamp, B. Polypropylene/SiO₂ nanocomposites with improved mechanical properties. *Rev. Adv. Mater. Sci.* **2004**, *6*, 169–175.
12. Grala, M.; Bartczak, Z.; Rózański, A. Morphology, thermal and mechanical properties of polypropylene/SiO₂ nanocomposites obtained by reactive blending. *J. Polym. Res.* **2016**, *23*, 25. [[CrossRef](#)]
13. Franciszczak, P.; Wojnowski, J.; Kalniņš, K.; Piesowicz, E. The influence of matrix crystallinity on the mechanical performance of short-fibre composites—Based on homo-polypropylene and a random polypropylene copolymer reinforced with man-made cellulose and glass fibres. *Compos. Part B* **2019**, *166*, 516–526. [[CrossRef](#)]
14. Wang, D.; Gao, J. Melting, nonisothermal crystallization behavior and morphology of polypropylene/random ethylene-propylene copolymer blends. *J. Appl. Pol. Sci.* **2006**, *99*, 670–678. [[CrossRef](#)]
15. Pereirah, J.R.D.; Bernardes, G.P.; Silv, J.A.P.; Bönmann, V.C.; Calcagno, C.I.W.; Santana, R.M.C. Structure-property correlation of an impact-modified random polypropylene copolymer. *J. Elastom. Plast.* **2021**, *53*, 450–468. [[CrossRef](#)]
16. Chapa-Rodriguez, R.; Avila de la Rosa, G.; Pérez, E. Thermal stability and ageing properties of PP-PE film modulated by nano-silica particles: Comparison between dry and moist particles. *Polym. Bull.* **2021**, *78*, 3071–3088. [[CrossRef](#)]
17. Rahman, I.A.; Vejayakumarana, P.; Sipaut, C.S.; Ismail, J.; Chee, C.K. Size-dependent physicochemical and optical properties of silica nanoparticles. *Mat. Chem. Physics* **2009**, *114*, 328–332. [[CrossRef](#)]
18. Alkan, Ü.; Karabul, Y.; Bulgurcuoğlu, A.E.; Kiliç, M.; Özdemir, Z.G.; İçelli, O. Polypropylene/basalt thick film composites: Structural, mechanical and dielectric properties. *e-Polymers* **2017**, *17*, 417–425. [[CrossRef](#)]
19. Hara, S.; Watanabe, S.; Takahashi, K.; Shimizu, S.; Ikake, H. Preparation of crystallites for oriented poly(lactic acid) films using a casting method under a magnetic field. *Polymers* **2018**, *10*, 1083. [[CrossRef](#)]
20. El Achaby, M.; Arrakhiz, F.E.; Voudreuil, S.; Qaiss, A.K.; Boushina, M.; Fassi-Fehri, O. Mechanical, thermal, and rheological properties of graphene-based polypropylene nanocomposites prepared by melt mixing. *Polym. Compos.* **2012**, *33*, 733–744. [[CrossRef](#)]
21. Tarani, E.; Arvanitidis, I.; Christofilos, D.; Bikiaris, D.N.; Chrissafis, K.; Vourlias, G. Calculation of the degree of crystallinity of HDPE/GNPs nanocomposites by using various experimental techniques: A comparative study. *J. Mater. Sci.* **2023**, *58*, 1621–1639. [[CrossRef](#)]
22. Blaine, R.L. Thermal Applications Note. Polymer Heats of Fusion. Available online: <https://www.tainstruments.com/pdf/literature/TN048.pdf> (accessed on 1 May 2024).
23. Pitsa, D.; Daniksa, M.G. Interfaces features in polymer nanocomposites: A review or proposed models. *NANO Brief Rep. Rev.* **2011**, *6*, 497–508. [[CrossRef](#)]
24. Kareem, S.; Al-Ansari, L.S.; Gömze, L.A. Modeling of modulus of elasticity of nano-composite materials: Review and evaluation. *J. Phys. Conf. Ser.* **2022**, *2315*, 012038. [[CrossRef](#)]
25. Majzoobil, G.H.; Malek-Mohammadi, H.; Payandehpeyman, J. A new cooperative model for the prediction of compressive yield stress of polycarbonate nanocomposites considering strain rate, temperature, and agglomeration. *J. Compos. Mater.* **2019**, *53*, 3567–3575. [[CrossRef](#)]
26. Delli, E.; Gkiliopoulos, D.; Vouvoudi, E.; Bikiaris, D.; Chrissafis, K. Defining the Effect of a Polymeric Compatibilizer on the Properties of Random Polypropylene/Glass Fibre Composites. *J. Compos. Sci.* **2024**, *8*, 44. [[CrossRef](#)]

Disclaimer/Publisher’s Note: The statements, opinions and data contained in all publications are solely those of the individual author(s) and contributor(s) and not of MDPI and/or the editor(s). MDPI and/or the editor(s) disclaim responsibility for any injury to people or property resulting from any ideas, methods, instructions or products referred to in the content.